IEEE Access
Multidisciplinary | Rapid Review | Open Access Journal

Received November 14, 2016, accepted November 22, 2016, date of publication December 15, 2016, date of current version January 27, 2017.

Digital Object Identifier 10.1109/ACCESS.2016.2640361

Photodetector Selection Aided Multiuser MIMO Optical OFDM Imaging Visible Light Communication System

KUNYI CAI[1], (Student Member, IEEE), MING JIANG[1,2], (Senior Member, IEEE), AND XIAO MA[1], (Member, IEEE)

[1]Sun Yat-sen University, Guangzhou 510006, China
[2]SYSU-CMU Shunde International Joint Research Institute, Foshan 528300, China

Corresponding author: M. Jiang (jiangm7@mail.sysu.edu.cn)

This work was supported in part by the Science and Technology Program Project of Guangdong Province under Grant 2016B090918109, in part by the Innovation Team Project of SYSU-CMU Shunde International Joint Research Institute under Grant 20150401, and in part by the Basic Research Project of Guangdong Provincial NSF under Grant 2016A030308008.

ABSTRACT While playing an important role in radio frequency (RF)-based wireless systems, multiple-input multiple-output (MIMO) techniques have also found viable applications in visible light communication (VLC) systems. However, how to effectively reduce the inherent strong correlations between optical MIMO channels remains a typical issue for VLC. In this paper, we propose an MIMO-aided multiuser optical orthogonal frequency division multiplexing VLC system employing an imaging receiver (ImR). The proposed new scheme efficiently mitigates the optical MIMO channel correlations across the multiple photodetectors (PDs) of the same user equipment (UE) or those between different UEs, through invoking a new technique called photodetector selection (PDS). Two possible PDS designs, namely random PDS and modified maximum minimum singular value PDS are investigated. Through both analytical analysis and numerical simulations, we show that the proposed PDS-aided ImR system is capable of outperforming its conventional non-imaging receiver and non-PDS ImR counterparts, especially when UEs are close to each other. Results demonstrate that the proposed system offers a stably low bit error rate in most areas of the room.

INDEX TERMS Imaging receiver (ImR), multiple-input multiple-output (MIMO), optical orthogonal frequency division multiplexing (OOFDM), photodetector selection (PDS), visible light communication (VLC).

I. INTRODUCTION

The use of light-emitting diodes (LEDs) provides an energy-efficient and environment-friendly way for human illumination. Visible light communication (VLC) systems utilise LEDs for simultaneous illumination and data communication, hence offering an exciting opportunity for a wide range of indoor services and attracting increasing interest across the globe [1]–[3]. In VLC systems, the binary information bits are mapped to symbols, which then modulate the intensity of the visible light emitted from LEDs. At the receiver side, photodetectors (PDs) are used for detecting the signals transmitted through optical channels. After the optical-to-electrical conversion, the received symbols are demodulated for recovering the bits. Since optical transmission is based on intensity modulation (IM) and direct detection (DD), real rather than complex signal processing is required in VLC systems [4]. Borrowing the concept of multiple-input multiple-output (MIMO) [5] technologies, in VLC systems arrays of multiple LEDs can be employed, which not only ensures sufficient illumination levels in modern indoor environment such as office buildings, shopping malls, etc., but also offers an opportunity to improve the achievable data rates. MIMO-VLC systems remove the bandwidth limitation of a single LED and provide an increased system throughput as well as spectral efficiency (SE).

In radio frequency (RF) based wireless communication scenarios, the spatial MIMO channel links are uncorrelated, if the spacing between antennas is sufficiently large. Otherwise, channel correlations may have an non-ignorable impact on the system design [6], [7]. In VLC scenarios, the channel gains between the LED and two closely-placed PDs are often similar, due to the fact that the line-of-sight (LOS)

transmission is dominant. Thus, the resultant high spatial correlation of indoor VLC channel links may severely degrade the systems' achievable performance. To reduce the channel correlation, measures such as increasing the distance between PDs, applying power imbalance, and even blocking selected channel links may be adopted [4]. For instance, power-imbalanced multiple transmit light sources are used to mitigate the high channel correlation imposed on conventional optical spatial modulation (OSM) schemes [8]. Others consider the employment of multiple PDs with different inclination angles on small mobile devices [9] or study the performance of angular-segmented full-mobility receivers [10]. Furthermore, the benefits of imaging receiver (ImR) are studied in [11], which help to achieve significant signal-to-noise ratio (SNR) gains [12]. An experimental indoor MIMO demonstration with ImR [13] and the design of a hemispherical lens based ImR system [14] also show the potential of ImR techniques in indoor MIMO-VLC applications. In addition, fisheye lens aided ImR may be used to provide an ultrawide field of view (FOV) [15]. It is also proposed to adopt an imaging angle diversity receiver to improve the system performance of indoor space division multiplexing assisted VLC systems [16].

Similar to RF systems, multiple user equipment (UE) may simultaneously be supported by VLC, resulting in multiuser (MU) VLC systems. For example, the optimisation problems for achieving minimum mean squared error (MMSE) and maximum sum-rate under power constraints for MU-VLC are investigated in [17] and [18], respectively. In [19], an MU-VLC transceiver design minimising the maximum mean squared error (MSE) is considered, while the framework of precoded MU-MIMO-VLC systems is described in [20] and [21]. Specifically, the need of reducing MIMO channel correlations is also applicable to MU-VLC systems [21]. For instance, utilising different FOV settings [21] and introducing angle diversity for PDs [22] in precoded MU-MIMO-VLC systems are among the potential solutions.

However, previous studies [20]–[22] on MU-VLC did not take into account the specific characteristics of VLC channels, PD configurations and/or spatial correlations between UEs. Against this background, in this paper we aim to jointly consider these aspects and propose to exploit the receiver diversity for mitigating the spatial correlations between MIMO channels. More specifically, by extending our previous work in [23], we elaborate on the full design details of an optical orthogonal frequency division multiplexing (OOFDM) based PD selection (PDS) assisted MU-MIMO indoor VLC system employing ImR, together with extensive simulation results and analyses. We will show that the proposed scheme is capable of significantly reducing VLC channel correlations between PDs of the same or different UEs, thus translating into a substantially enhanced stable link performance in typical indoor scenarios.

The organisation of this paper is as follows. The proposed system model is illustrated in Section II-A, followed by the bit error rate (BER) performance analysis in Section II-B. The ImR and PDS designs are then given in Section II-C. Furthermore, we discuss the complexity issues in Section II-D. Our simulation results and analyses are provided in Section III, where the system performances are revealed and compared from different aspects. Finally, Section IV concludes our findings.

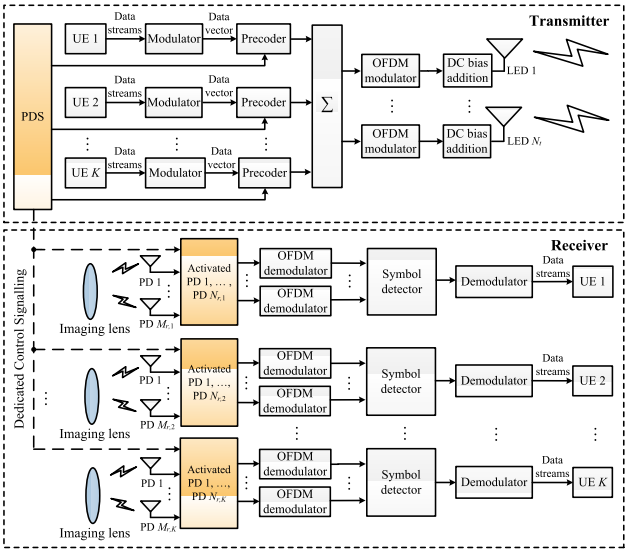

FIGURE 1. Block diagram of the proposed system.

II. SYSTEM MODEL

Fig. 1 shows the schematic of the proposed PDS aided MU-MIMO-OOFDM-ImR-VLC system operating in a typical indoor scenario, assuming N_t LED arrays and K UEs. The j^{th} UE is equipped with $M_{r,j}$ PDs, implying a total number of $M_r = \sum_{j=1}^{j=K} M_{r,j}$ PDs in the system. At a time, only $N_{r,j}$ out of the $M_{r,j}$ PDs are activated for signal processing at the j^{th} UE. Hence, the total number of activated PDs in the system is $N_r = \sum_{j=1}^{j=K} N_{r,j}$.

A. MU-PRECODED MIMO-OOFDM-VLC MODEL

We consider a downlink VLC system employing the block diagonalisation precoder (BDP) of [24]. The number of data streams q_j targeting the j^{th} UE should satisfy $q_j \leq N_{r,j} (j = 1, \ldots, K)$ and $\sum_{j=1}^{j=K} q_j \leq N_t$, which are necessary conditions for BDP operations [25]. Aiming at maximising the spatial degree of freedom, we assume $\sum_{j=1}^{j=K} q_j = N_t$ and $N_{r,j} = q_j (j = 1, \ldots, K)$. Thus, each UE sees an $(N_t \times N_{r,j})$ MIMO configuration delivering $N_{r,j}$ data streams, and we have $N_r = \sum_{j=1}^{j=K} N_{r,j} = N_t$.

The solving process of BDP is briefed as follows. First, we define an $((N_r - N_{r,j}) \times N_t)$ channel matrix as $\tilde{\mathbf{H}}_j = [\mathbf{H}_1^H, \ldots, \mathbf{H}_{j-1}^H, \mathbf{H}_{j+1}^H, \ldots, \mathbf{H}_K^H]^H$, where $\mathbf{H}_k$ $(k = 1, \ldots, j-1, j+1, \ldots, K)$ is the $(N_{r,k} \times N_t)$ channel matrix for the k^{th} UE. Then we calculate the singular value

decomposition (SVD) [26] of $\tilde{\mathbf{H}}_j$ by

$$\tilde{\mathbf{H}}_j = \tilde{\mathbf{U}}_j \tilde{\Lambda}_j [\tilde{\mathbf{V}}_j^{(1)} \mid \tilde{\mathbf{V}}_j^{(0)}]^H, \tag{1}$$

where the $((N_r - N_{r,j}) \times (N_r - N_{r,j}))$ matrix $\tilde{\mathbf{U}}_j$ contains left singular vectors, the $((N_r - N_{r,j}) \times N_t)$ matrix $\tilde{\Lambda}_j$ is formed by ordered singular values of $\tilde{\mathbf{H}}_j$, the $(N_t \times \tilde{L}_j)$ matrix $\tilde{\mathbf{V}}_j^{(1)}$ holds the first $\tilde{L}_j$ right singular vectors with $\tilde{L}_j$ being the rank of $\tilde{\mathbf{H}}_j$, and the $(N_t \times (N_t - \tilde{L}_j))$ matrix $\tilde{\mathbf{V}}_j^{(0)}$ forms the orthogonal basis for the null space of $\tilde{\mathbf{H}}_j$. Generally, when the channel matrix is row full rank, we have $N_t - \tilde{L}_j = N_{r,j}$. Then applying SVD yields

$$\bar{\mathbf{H}}_j = \mathbf{H}_j \tilde{\mathbf{V}}_j^{(0)} = \mathbf{U}_j \Lambda_j \mathbf{V}_j^{(1)H}, \tag{2}$$

where Λ_j is an $(N_{r,j} \times N_{r,j})$ diagonal matrix containing the singular values, the $(N_{r,j} \times N_{r,j})$ unitary matrix $\mathbf{U}_j$ is the decoding matrix, and $\mathbf{V}_j^{(1)}$ is the $(N_{r,j} \times N_{r,j})$ matrix of right singular vectors assuming full rank. Then, we can obtain the $(N_t \times N_{r,j})$ precoding matrix $\mathbf{P}_j$ for the j^{th} UE

$$\mathbf{P}_j = [\mathbf{p}_{1,j}^T, \ldots, \mathbf{p}_{N_t,j}^T]^T = \tilde{\mathbf{V}}_j^{(0)} \mathbf{V}_j^{(1)}, \tag{3}$$

where $\mathbf{p}_{i,j}$ is the $(1 \times N_{r,j})$ i^{th} row vector of $\mathbf{P}_j$.

If we denote $\mathbf{u}_j^{(l)}$ as the $(N_{r,j} \times 1)$ bipolar on-off-keying (OOK) data vector transmitted at the l^{th} subcarrier for the j^{th} UE, the $(N_t \times 1)$ precoded signals $\mathbf{f}^{(l)}$ are

$$\mathbf{f}^{(l)} = [f_1^{(l)}, \ldots, f_{N_t}^{(l)}]^T = \sum_{j=1}^{K} \left(\mathbf{P}_j \mathbf{u}_j^{(l)}\right), \tag{4}$$

which will be forwarded to the OOFDM modulator seen in Fig. 1. As an example, in this paper we adopt the direct-current biased optical OFDM (DCO-OFDM) [27], where a DC bias is added to the signal before the clipping operation is invoked. The required DC bias for the i^{th} LED array is denoted by

$$B_{\mathrm{DC},i} = \xi \sqrt{(E\{x_{0,i}^2(t)\})}, \tag{5}$$

where $x_{0,i}(t)$ is the time domain (TD) signal and ξ is a proportionality parameter defined as a bias of $10\log_{10}(\xi^2 + 1)$ [dB] [27]. Then, the TD signal to be transmitted from the i^{th} LED becomes $x_i(t) \approx x_{0,i}(t) + B_{\mathrm{DC},i}$. Furthermore, at a given DC bias level of for example 7dB or 13dB, the optical powers of the LEDs also vary due to different bias values required to minimise the impact from clipping. In order to maintain a uniform illumination level and minimise the clipping noise, we may apply the maximal required DC bias value to all LED arrays. This yields the same emitted optical power

$$I_0 \approx B_{\mathrm{DC,max}} = \max(B_{\mathrm{DC},1}, \ldots, B_{\mathrm{DC},N_t}). \tag{6}$$

Usually, the LOS component of the indoor VLC channel is much stronger than diffuse components. For simplicity, in this paper we only consider the LOS transmission as in [4] and [11] and assume the channel is frequency flat at each subcarrier. Then at the receiver we have

$$\mathbf{y} = R\mathbf{H}\mathbf{x} + \mathbf{n}, \tag{7}$$

where $\mathbf{y}$ is the $(N_r \times 1)$ received signal, $\mathbf{x} = (x_1(t), \ldots, x_{N_t}(t))^T$ is the transmitted optical signal, $\mathbf{n}$ is the additive white Gaussian noise (AWGN), R is the PD responsivity, and the $(N_r \times N_t)$ MIMO channel matrix is

$$\mathbf{H} = \begin{pmatrix} h_{11} & \cdots & h_{1N_t} \\ \vdots & \ddots & \vdots \\ h_{N_r 1} & \cdots & h_{N_r N_t} \end{pmatrix}, \tag{8}$$

where h_{pi} is the optical channel link between the p^{th} PD and the i^{th} LED. Note that the statistics of the optical channel links are related to a number of factors, including the positions of LEDs and receivers, as well as the type of receiver such as ImR or non-imaging receiver (NImR), etc. After OOFDM demodulation, the equivalent received signal at the l^{th} subcarrier at the j^{th} UE is

$$\mathbf{r}_j^{(l)} = R\mathbf{U}_j \Lambda_j \mathbf{u}_j^{(l)} + \mathbf{n}_j, \tag{9}$$

where $\mathbf{n}_j$ is the AWGN vector associated with the j^{th} UE. Finally, we can obtain the $(N_{r,j} \times 1)$ estimated signal vector at the l^{th} subcarrier for the j^{th} UE

$$\hat{\mathbf{u}}_j^{(l)} = \mathbf{U}_j^H \mathbf{r}_j^{(l)} = R\Lambda_j \mathbf{u}_j^{(l)} + \mathbf{U}_j^H \mathbf{n}_j. \tag{10}$$

B. BER PERFORMANCE ANALYSIS

We define SNR as a modulation-independent general form of $\gamma = \frac{I^2}{\sigma^2}$ as in [4], where I is the total emitted mean optical power of all LEDs and σ^2 is the AWGN power. Assuming uniform illumination, we have $I = N_t I_0$, where I_0 is given in (6). Since the common VLC channel gains are at an order of 10^{-6}, in the above SNR definition, an offset of at least 120dB exists over the receive SNR.

According to (10), at each subcarrier, the symbol in the q^{th} data stream is recovered at the q^{th} PD in the electrical domain. Thus, the per-subcarrier BER of the j^{th} UE can be derived from the BER of bipolar OOK in AWGN [28], as

$$\mathrm{BER}_j = \frac{1}{N_{r,j}} \sum_{q=1}^{N_{r,j}} Q\left(\sqrt{\frac{2R^2 \lambda_{j,q}^2 E\{u_{j,q}^2\}}{\sigma^2}}\right), \tag{11}$$

where $Q(x) = \int_x^\infty \frac{1}{\sqrt{2\pi}} e^{-\frac{y^2}{2}} dy$, while $\lambda_{j,q}$ and $E\{u_{j,q}^2\}$ denote the singular value in Λ_j and the average electrical power of the bipolar OOK symbols on the q^{th} data stream for the j^{th} UE, respectively. Note that for notation simplicity, we have omitted the subcarrier index l in (11). Furthermore, if the DC bias is sufficiently high, the effect of clipping noise in DCO-OFDM can be neglected and thus is not considered in (11).

Next, to better reflect the VLC system's characteristics, (11) should also take into account the DC consumption inflicted by OOFDM. Without loss of generality, we assume that each data stream is applied a uniform electrical power, namely $E\{u_{j,q}^2\} = a$ $(q = 1, \ldots, N_{r,j};\ j = 1, \ldots, K)$. Recalling the precoded signal $\mathbf{f}$ for the LED arrays defined by (4), the average electrical power of f_i associated with

$\mathbf{P}_j (j = 1, \ldots, K)$ can be given by

$$E\{f_i^2\} = \sum_{j=1}^{j=K} \mathbf{p}_{i,j}\mathbf{p}_{i,j}^H \cdot a = Z_i \cdot a, \tag{12}$$

where $Z_i = \sum_{j=1}^{j=K} \mathbf{p}_{i,j}\mathbf{p}_{i,j}^H$. In DCO-OFDM, given that $E\{x_{0,i}^2(t)\} = E\{f_i^2\}$ and that the maximum required DC bias will be applied to all LED arrays, we have

$$B_{\mathrm{DC,max}} = \xi\sqrt{\max(E\{f_1^2\}, \ldots, E\{f_{N_t}^2\})}. \tag{13}$$

By exploiting (6) and (13), the total emitted optical power can be written as

$$\begin{aligned} I &= N_t I_0 \\ &\approx N_t \xi \sqrt{\max(E\{f_1^2\}, \ldots, E\{f_{N_t}^2\})} \\ &= N_t \sqrt{\max(Z_1, \ldots, Z_{N_t})\xi^2 a} \\ &= N_t \sqrt{\nu a}, \end{aligned} \tag{14}$$

where we define the DC consumption coefficient as $\nu = \max(Z_1, \ldots, Z_{N_t})\xi^2$. Hence, combining (14) and the definition of γ, (11) can be rewritten as

$$\mathrm{BER}_j = \frac{1}{N_{r,j}} \sum_{q=1}^{N_{r,j}} Q\left(\sqrt{\frac{2R^2\lambda_{j,q}^2\gamma}{N_t^2\nu}}\right). \tag{15}$$

From (15), we note that both the DC consumption coefficient ν and the singular values $\lambda_{j,q}$ have an impact on the achievable BER.

C. IMAGING RECEIVER INVOKING PDS

In NImR systems, the received signal is a superimposed version of the optical signals transmitted from all LED arrays. In this case, it may result in high channel correlations between adjacent PDs. In contrast, an ImR system exploits the imaging lens to separate the optical signals in free space, hence becomes an effective solution for decoupling the correlation between VLC channel links and offers notable spatial diversity.

For a given position in the room, we denote the elements of the MIMO VLC channel matrix $\mathbf{H}$ as h_{pi}, which represent the optical links between the p^{th} PD and the i^{th} LED array [29]

$$h_{pi} = h_i^{\mathrm{fs}} h_{pi}^{\mathrm{im}}, \tag{16}$$

where h_i^{fs} is the free-space channel gain between the i^{th} LED array and the aperture of the imaging lens, while h_{pi}^{im} is the imaging channel gain between the i^{th} LED array and the p^{th} PD. If the full image of a LED array can be projected onto the PDs via lens, we have [29]

$$h_i^{\mathrm{fs}} = \frac{(m+1)A_0 cos^m(\phi_i)}{2\pi D_i^2} T_s(\psi_i) g(\psi_i) cos(\psi_i), \tag{17}$$

where the variables have the same meaning as defined in [29].

In the three-dimensional system coordinate system (SCS) $(\bar{x}, \bar{y}, \bar{z})$ shown in Fig. 2, where $\bar{x}$, $\bar{y}$ and $\bar{z}$ denote the SCS coordinate units, the origin is set to be at the centre of the room's floor, denoted by $\mathcal{O}(\bar{x}, \bar{y}, \bar{z}) = (0, 0, 0)$. The positions of LED arrays and UEs are represented by the positions of their geometric centres with respect to SCS, respectively. Moreover, it is assumed that the imaging lens of the ImR is placed in the middle of the UE, and is shared by the UE's several PDs. Note that the signals transmitted from LED arrays may be projected to one or more PDs through the imaging lens. In the example shown in Fig. 2, the points forming the image on the PD, namely A', B', C' and D', correspond to the points A, B, C and D forming the LED array, respectively. Furthermore, we also define a PD coordinate system (PCS) $(\hat{x}, \hat{y}, \hat{z})$ with $\hat{x}$, $\hat{y}$ and $\hat{z}$ denoting the PCS coordinate units, whose origin is set to be at the centre of the imaging lens associated with a set of PDs, as seen in Fig. 2.

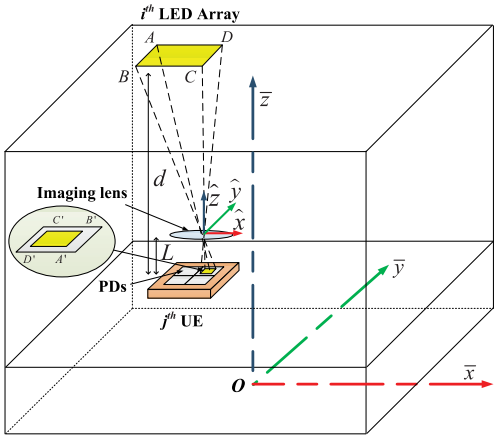

FIGURE 2. Illustration of the ImR model in the proposed system.

Assuming the use of paraxial optical lens, the image formed by the lens can be geometrically distortionless in comparison to the source [11]. The magnification coefficient M is given by [11]

$$M = \frac{L}{d - L}, \tag{18}$$

where L is the focal length of the imaging optics and d is the vertical distance from the receiving plane to the ceiling, as indicated in Fig. 2.

Let $\mathbf{C}_t = (x_t\bar{x}, y_t\bar{y}, z_t\bar{z})$ and $\mathbf{C}_r = (x_r\bar{x}, y_r\bar{y}, z_r\bar{z})$ be the SCS positions of the LED array and the imaging lens, respectively. We also define

$$\mathbf{d} = (d_x\bar{x}, d_y\bar{y}, d_z\bar{z}) = \mathbf{C}_t - \mathbf{C}_r \tag{19}$$

as the vector from $\mathbf{C}_r$ to $\mathbf{C}_t$. Noting that the PCS origin is at the centre of the imaging lens, the centre of the image projected by the i^{th} LED array can therefore be expressed as

$$\mathbf{C}_{\mathrm{im},i} = (-Md_x\hat{x}, -Md_y\hat{y}, -L\hat{z}). \tag{20}$$

Then, h_{pi}^{im} in (16) can be derived by

$$h_{pi}^{\mathrm{im}} = \frac{\eta_{i_p}}{\alpha_i} = \frac{\alpha_i \bigcap \beta_p}{\alpha_i}, \tag{21}$$

where α_i is the area of the image associated with the i^{th} LED array and formed by the lens, β_p is the area of the p^{th} PD, and η_{i_p} is the part cast on β_p by α_i.

Note in the case that when the image falls onto too few PDs, implying a very small η_{i_p}, due to for example an excessively large angle of incidence, blind spots might appear where the performance of the ImR system is significantly degraded because of the very low receive SNR level. This could happen when, for instance, the UE is located far from the LED arrays in a very large room. However, such a negative effect can be minimised by selecting an appropriate number of LED arrays and mounting them to proper positions on the ceiling, thus avoiding large angles of incidence. Another issue is that when multiple UEs are at the same far-end side of the LED arrays and are close to each other, it may lead to outage of conventional, especially ImR VLC systems. More specifically, in this case the channel correlation between the UEs becomes very high, due to the non-full-rank overall MIMO channel matrix induced by those UEs' adjacent locations far from the LED arrays. Nonetheless, by employing our proposed PDS technique to be detailed in the sequel, we may not only further reduce the channel correlation between the UEs, but also improve the robustness of VLC transmissions by minimising the occurrence of outage probability, as will be demonstrated in Section III.

More specifically, different from conventional MU-MIMO-VLC systems using BDP, where $M_{r,j} = N_{r,j} = q_j$ is a typical assumption, in the PDS scheme only some of the PDs are activated at one time, implying $M_{r,j} > N_{r,j} = q_j$. Hence, in the proposed PDS-aided MU-MIMO-VLC system, the overall MIMO configuration becomes $(N_t \times [N_{r,1}, \ldots, N_{r,K}])$ after the PDS operation. As mentioned in Section II-A, the required number of PDs to be activated, namely $N_{r,j}$, is determined by the number of LED arrays and the supported number of data streams.

There can be different PDS strategies. In the simple random PD selection (R-PDS) scheme, $N_{r,j}$ number of PDs are randomly chosen from $M_{r,j}$ PDs at the j^{th} UE under the BDP constraints. Naturally, R-PDS is unable to achieve the optimal performance due to its random nature. Thus, another strategy adopting a new metric originating from the maximum minimum singular value [30] (MMSV) criterion is considered, which is referred to as the modified MMSV based PD selection (mMMSV-PDS). As shown in [31], the receive SNR of single-user (SU) spatial multiplexing (SMP) systems with linear receivers is lower bounded by the monotonically increasing function of the minimum singular value (MSV) of the equivalent channel. On the other hand, the maximum system BER of MU systems is upper bounded by the UE with the worst performance. According to (15), the j^{th} UE's performance is related to the minimum value of $\frac{\lambda_{j,q}^2}{\nu}$ $(q = 1, \ldots, N_{r,j})$. More specifically, the achievable BER performance is associated with not only the singular values of the channel, but also the DC consumption coefficient ν introduced by DCO-OFDM. This is a case different from conventional RF-based MU systems in that given a fixed transmit power budget, the higher DC consumption, the less remaining power available for the payload, which thus degrades the achievable system performance.

Based on the above analysis, we summarise the proposed mMMSV-PDS scheme as follows.

Step 1: Create a candidate set m_p corresponding to the full-rank overall channel matrix under the BDP constraints and containing $N_{r,j}$ $(j = 1, \ldots, K)$ activated PDs for each UE, where we have $m_p \in \Omega_p$ and Ω_p is the set of all M_r PDs in the system.

Step 2: For every candidate subset m_p, compute the SVD of $\mathbf{H}_{j,m_p}\tilde{\mathbf{V}}_{j,m_p}^{(0)}(j = 1, 2, \ldots, K)$ by

$$\mathbf{H}_{j,m_p}\tilde{\mathbf{V}}_{j,m_p}^{(0)} = \mathbf{U}_{j,m_p}\Lambda_{j,m_p}\mathbf{V}_{j,m_p}^{(1)H}, \tag{22}$$

where $\mathbf{H}_{j,m_p}$ and $\tilde{\mathbf{V}}_{j,m_p}^{(0)}$ are the j^{th} UE's channel matrix associated with m_p and the corresponding right singular vector generated by (1), respectively. Then we get the MSV of the j^{th} UE for a given m_p as

$$\lambda_{j,m_p}^{\min} = \min\left\{\mathrm{diag}(\Lambda_{j,m_p})\right\}, \tag{23}$$

where $\mathrm{diag}(\Lambda_{j,m_p})$ is the operation that forms a set containing all elements on the diagonal of Λ_{j,m_p}. Next, we compute

$$\tilde{\kappa}_{m_p}^{\min} = \min_{j=1,\ldots,K} \frac{(\lambda_{j,m_p}^{\min})^2}{\nu_{m_p}}, \tag{24}$$

where $\tilde{\kappa}_{m_p}^{\min}$ denotes the minimum ratio of the second power of a UE's MSV and the DC consumption coefficient ν_{m_p} for a given m_p.

Step 3: Select the PD set m_p that satisfies

$$m_{p,\mathrm{solution}} = \underset{m_p \in \Omega_p}{\mathrm{argmax}}\{\tilde{\kappa}_{m_p}^{\min}\}, \tag{25}$$

which is considered as the solution PD subset to be activated at the corresponding UEs. In either R-PDS or mMMSV-PDS, we finally obtain a full-rank $(N_r \times N_t)$ channel matrix $\mathbf{H}$.

In this work, we assume that perfect channel state information (CSI) is available at the transmitter side. Similar to conventional RF-based wireless systems, the CSI can be obtained either through feedbacks from the UE in frequency division duplexing (FDD) mode, or by channel estimation at the transmitter in time division duplexing (TDD) mode. Since it may not be desirable for the UE to emit visible light, infrared communication techniques can be employed in the uplink [32]. Furthermore, as the PDS function is applied at the transmitter side, the information of selected PDs needs to be signalled to the UEs. This may be achieved through a dedicated control channel like physical downlink control channel (PDCCH) in long-term evolution (LTE) networks. Alternatively, a fixed PD-hopping pattern may be employed as a pseudo-random approach for signaling overhead reduction at the cost of some performance degradation, in order to strike for a practical tradeoff in engineering implementations.

D. COMPLEXITY ANALYSIS

In the proposed mMMSV-PDS scheme, since the number of candidate activated PD sets for the j^{th} UE is $C_{M_{r,j}}^{N_{r,j}}$, there are a total of $\prod_{j=1}^{j=K} C_{M_{r,j}}^{N_{r,j}}$ such candidate sets, where C_m^n represents an n-combination of the set that has m elements. On the selection of a set m_p, the associated computational complexity mainly results from $2K$ SVD operations and K matrix multiplications, which can be measured by the number of flops. For convenience, according to (22), we denote the required numbers of flops for invoking SVD to get $\tilde{\mathbf{V}}_{j,m_p}^{(0)}$, for the calculation of the matrix product $\mathbf{H}_{j,m_p}\tilde{\mathbf{V}}_{j,m_p}^{(0)}$ and for invoking SVD to get Λ_{j,m_p} as a_j, b_j and c_j, respectively. Note that in VLC systems the above-mentioned operations are applied on real matrices, and the multiplication of an $(A \times B)$ real matrix with a $(B \times C)$ real matrix requires $2ABC$ flops. In the SVD operation on an $(A \times B)$ matrix, if counting multiplication operations only and ignoring the addition operations, it requires about $(9A^3 + 8A^2B + 4AB^2)$ flops [33]. Hence, since the number of candidate activated PD sets that satisfy the full-rank assumption is always equal to or less than $\prod_{j=1}^{j=K} C_{M_{r,j}}^{N_{r,j}}$, the required number of flops χ characterising the associated computational complexity may be formulated as

$$\begin{aligned}\chi &\le \Big(\prod_{j=1}^{j=K} C_{M_{r,j}}^{N_{r,j}}\Big)\Big[\sum_{j=1}^{j=K}(a_j + b_j + c_j)\Big] \\ &= \Big(\prod_{j=1}^{j=K} C_{M_{r,j}}^{N_{r,j}}\Big)\Big[\sum_{j=1}^{j=K}(9\tilde{N}_{r,j}^3 + 8\tilde{N}_{r,j}^2 N_t + 4\tilde{N}_{r,j}N_t^2 \\ &\qquad + 2N_{r,j}^2 N_t + 21N_{r,j}^3)\Big], \end{aligned} \tag{26}$$

where we define $\tilde{N}_{r,j} = N_r - N_{r,j}$.

From (26) we note that a larger value of $C_{M_{r,j}}^{N_{r,j}}$ $(j = 1, \ldots, K)$ and/or a higher number of UEs K result in a quickly increasing computational complexity. Therefore, we suggest that the values of these parameters should be restricted to avoid an excessive implementational cost.

III. SIMULATION RESULTS AND DISCUSSIONS

We consider an MU-MIMO-OOFDM-VLC system with $N_t = 4$ LED arrays and $K = 2$ UEs. The four LED arrays are mounted near the corners of the ceiling, as shown in Fig. 3. We assume that the number of data streams for the j^{th} UE is $q_j = 2$ $(j = 1, 2)$, and each UE is equipped with a (2×2) square array of PDs. Based on the BDP constraints and assumptions in Section II-A, 2 out of 4 PDs at each UE should be selected and activated during one symbol duration. If the receiver contains a higher number of PDs, the proposed PDS principle can still apply. For comparison, we also consider a conventional system setup dispensing with PDS, where each UE exploits a (1×2) array of PDs that are always fully activated. In either case, we have a $(4 \times [2, 2])$ MU-MIMO imaging VLC system, where 1024 OOFDM subcarriers are employed. Furthermore, the pitch between two adjacent PDs

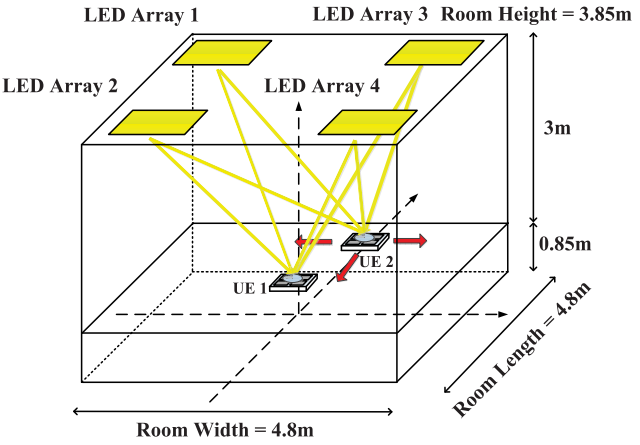

FIGURE 3. The room model used in the simulations.

TABLE 1. The major simulation parameters used.

Parameters	Value
Room size	$4.8\text{m} \times 4.8\text{m} \times 3.85\text{m}$
Number of LED arrays, N_t	4
Positions of LED arrays	(-2,2,3.85), (-2,-2,3.85), (2,2,3.85), (2,-2,3.85)
Number of UEs, K	2
Number of streams per UE, $q_j, j = 1, 2$	2
LED array size	$60\text{cm} \times 60\text{cm}$
Detector area of PD, A	1cm^2
Transmitter semi-angle, ϕ	60°
DC bias level	13dB, unless otherwise stated
PD responsivity, R	1.0A/W
Focal length, L	0.6cm
Optical FOV	70°
PD pitch	1.01cm

is 1.01cm, while each PD's physical area is $1\text{cm} \times 1\text{cm} = 1\text{cm}^2$. To have a fair comparison with the NImR benchmark system, the aperture of the proposed ImR system is modelled in a way, such that it has an area of 1cm^2 to ensure that the same incident signal radiant flux applies to both systems. The major parameters are summarised in Table 1.

As the first example, we consider Scenario A, where UE 1 is fixed at the SCS origin or equivalently the middle of the room, while UE 2 takes three different positions P-A1, P-A2 and P-A3, respectively, as shown in Fig. 4(a). Fig. 5 shows both the theoretical BER calculated by (15) and the simulated performances of various indoor MU-MIMO-OOFDM-VLC systems, as well as the performances of the conventional NImR and ImR benchmarkers without PDS. As observed in Fig. 5, the theoretical and simulated results match well, since a 13dB DC bias is utilised to eliminate the clipping noise. Furthermore, at a BER of 10^{-5}, for instance, the ImR system outperforms its NImR counterpart by about 45dB, 48dB and 48dB at P-A1, P-A2 and P-A3, respectively. This indicates that the application of imaging lens helps to reduce the channel correlation among the PDs of the same or different UEs, and thus provides a high spatial diversity for the MU-MIMO-VLC system, exhibiting the advantages of ImR based VLC system over its NImR counterpart. Moreover, if R-PDS is invoked in the ImR system, a further SNR gain of about 15dB can be achieved at P-A1 in comparison to

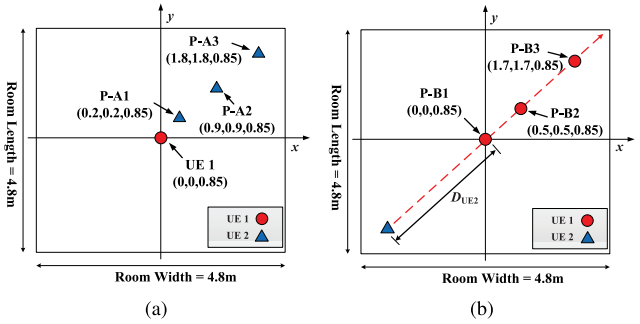

FIGURE 4. **The configurations of UE positions in Scenarios A and B. (a) Scenario A: UE 1 fixed; UE 2 fixed at different positions. (b) Scenario B: UE 1 fixed; UE 2 moving.**

the non-PDS ImR system, as shown in Fig. 5. However, the performance benefit of R-PDS vanishes or even becomes negative at P-A2 and P-A3, due to its non-optimal design that cannot adapt to the various channel states at different UE positions. In contrast, the mMMSV-PDS ImR scheme outperforms the non-PDS ImR system by about 16dB, 5dB and 3dB in terms of SNR gain at P-A1, P-A2 and P-A3, respectively. Moreover, Fig. 5 reveals that if the proposed mMMSV-PDS technique is incorporated into the conventional NImR system, the achievable system performance can be improved by about 0.4dB, 3dB and 9dB SNR gains at P-A1, P-A2 and P-A3, respectively.

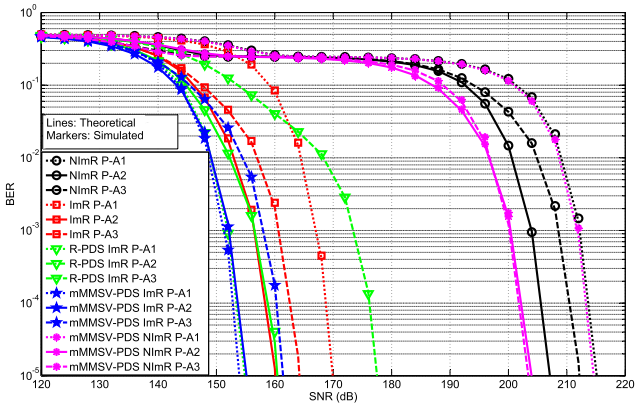

FIGURE 5. **BER performance comparison of MU-MIMO-OOFDM-VLC systems.**

Hence, we conclude that in most cases, the mMMSV-PDS scheme can indeed substantially enhance the attainable performances of the MU-MIMO-VLC system without or with imaging lens. Such benefits can be achieved, thanks to the optimally activated PDs recommended by the mMMSV algorithm, which is capable of reducing the MU-MIMO-VLC channel correlations between UEs, especially when two UEs are close to each other, for instance at P-A1 seen in Fig. 4(a). Even in the case where the UEs are separated relatively far apart as at P-A2 or P-A3, the mMMSV-PDS scheme can still provide some gains, as revealed by Fig. 5. Generally speaking, the mMMSV-PDS aided ImR system provides the best achievable overall performance among all systems evaluated.

Note specifically that although R-PDS can improve the achievable performance for two close-by UEs at P-A1, it may also introduce even worse channel correlations when the UEs are separated farther. In contrast, the property of mMMSV-PDS is particularly attractive, since it can attain positive gains across most UE positions in the room. Furthermore, the results in Fig. 5 also imply that the characteristics of the indoor VLC channel are quite different from those of RF channels. More explicitly, unlike RF systems that are typically studied in macroscopically statistical channels, the performance of VLC systems is determined by the more or less microscopic channel conditions associated with a number of aspects, such as the specific positions of LEDs and UEs.

To have a deeper insight into the proposed system, we further investigate the performance impact from different UE positions in Scenario B, as illustrated in Fig. 4(b). More specifically, in this testing scenario, UE 1 is assumed to be fixed at three given positions, denoted by P-B1, P-B2 and P-B3, respectively. On the other hand, we assume that UE 2 moves along the diagonal of the room, where the distance between UE 2 and the room centre is denoted by D_{UE2}. The increase of D_{UE2} from negative to positive values implies that UE 2 moves from the bottom-left to the top-right corner of the room.

Fig. 6 depicts the minimum SNR values required for achieving the target BER of 10^{-5} under different D_{UE2} values, when UE 1 takes the three positions specified in Fig. 4(b), respectively. Firstly, as expected, the conventional NImR system requires a much higher minimum SNR than ImR systems, as it suffers from a high MIMO channel correlation that corrupts the received signals. Furthermore, the performances of both the NImR and the conventional ImR systems become worse, when the two UEs are getting closer to each other and thus result in an increased correlation between the channels of the UEs. Particularly, under the conventional ImR scheme without PDS, a system outage may occur, when both UEs are closely located to the same far-end side of the LED arrays, as indicated by the vertical part of the ImR curve in Fig. 6(c). In this case, the ImR system is no longer able to satisfy the target BER of 10^{-5}. In contrast, the ImR aided systems employing either PDS technique are capable of offering decent performances even when both UEs become very close, as seen from all cases in Fig. 6. Furthermore, it is worth mentioning that despite the fact that the NImR system may also benefit from the proposed mMMSV-PDS technique, the inherent characteristics of the NImR mechanism largely constrains the overall achievable performance even with the aid of mMMSV-PDS. Hence, we can see that it is the integration of ImR and mMMSV-PDS that fully elevates the potentials of MU-MIMO-VLC systems. As observed in Fig. 6, among all schemes tested, the mMMSV-PDS aided ImR system achieves the best and the most robust performance in the majority of the test cases, regardless of the position of UE 1. Hence, the proposed mMMSV-PDS aided ImR system not only attains a

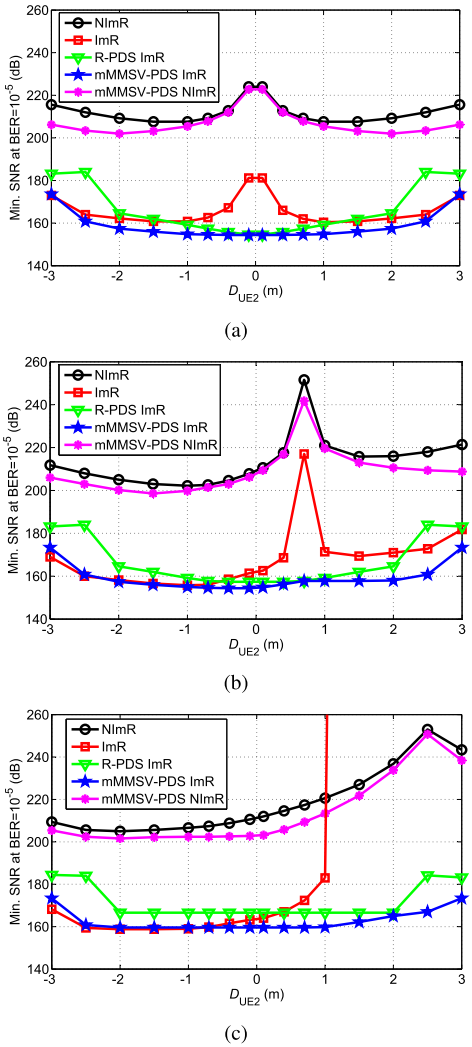

FIGURE 6. Minimum SNR required for achieving the target BER of 10^{-5} as a function of D_{UE2} in various MU-MIMO-OOFDM-VLC systems. (a) Scenario B: UE 1 at P-B1; UE 2 moving. (b) Scenario B: UE 1 at P-B2; UE 2 moving. (c) Scenario B: UE 1 at P-B3; UE 2 moving.

significant performance enhancement to conventional schemes, but also mitigates the aforementioned UE-position-related outage problem induced by the ImR mechanism, as discussed in Section II-C.

In Fig. 7(a) and Fig. 7(b), we show the full-room BER distributions of the conventional ImR and the proposed mMMSV-PDS aided ImR systems as a function of UE 2's position, respectively, under a fixed overall transmit SNR of 153dB. We assume that UE 1 is fixed at two positions, namely P-B1 and P-B2 of Fig. 4(b), respectively, while UE 2 moves around in the entire room. As observed in Fig. 7(a), the system tends to perform worse when UE 2 is in the vicinity of UE 1, since the multiuser interference (MUI) cannot be sufficiently mitigated due to the highly correlated channels between the two UEs. In contrast, the proposed mMMSV-PDS aided system is capable of selecting appropriate PDs to ensure low channel correlations, and thus

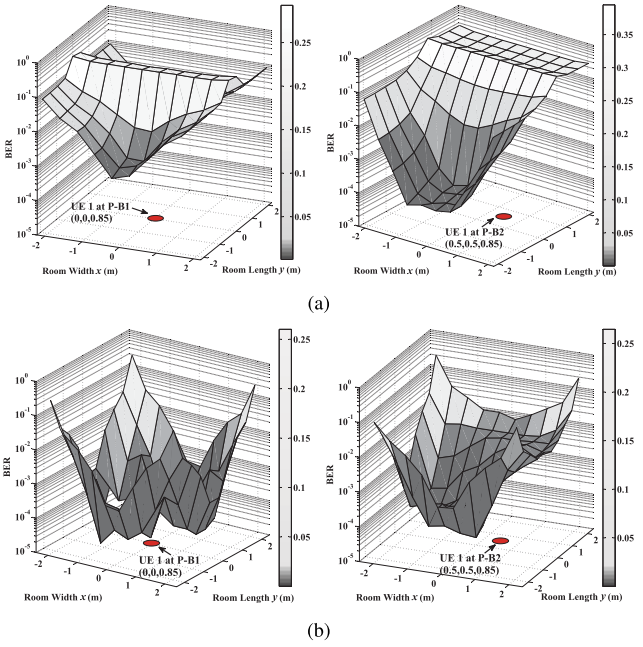

FIGURE 7. BER comparison of the ImR-MU-MIMO-OOFDM-VLC systems with and without PDS, as a function of UE 2's position in the entire room. (a) Performance of the ImR-MU-MIMO-OOFDM-VLC system. (b) Performance of the mMMSV-PDS aided ImR-MU-MIMO-OOFDM-VLC system.

significantly reducing the high BER floors across most areas of the room, as exhibited in Fig. 7(b).

Last but not least, in Fig. 8 we evaluate the impact from the DC bias level on the proposed system, which is related to the clipping distortion on VLC signals. Different from conventional RF OFDM systems where the transmitted signals are complex, the achievable system performance of OOFDM systems is constrained by the DC bias level. More explicitly, the lower DC bias, the higher non-linear clipping distortion is introduced, which may significantly degrade the OOFDM system's performance [34]. In Fig. 8, which corresponds to the so-called Scenario C, we assume that UE 1 is fixed at P-B1, while UE 2 takes the positions of P-A1 and P-B3, respectively. Similar to Fig. 5, the theoretical BER curves in Fig. 8 are also plotted by using (15).

One one hand, when the two UEs are separated far apart, namely UE 1 at P-B1 and UE 2 at P-B3, we note that the BER decreases as the DC bias decreases, which is an expected trend. More explicitly, under a given transmit SNR budget, although a reduced DC bias increases the clipping noise, it also saves more transmit power to be used for the payload, which then improves the receive SNR and so the BER performance. Furthermore, recall that (15) is derived without considering the contribution from the clipping noise. However, within the DC bias range tested in Fig. 8, the simulated BERs match well with theoretical results. This implies that in this case, where both UEs are far from each other, the clipping noise corresponding to the DC bias values evaluated does not have an obvious impact on the system performance.

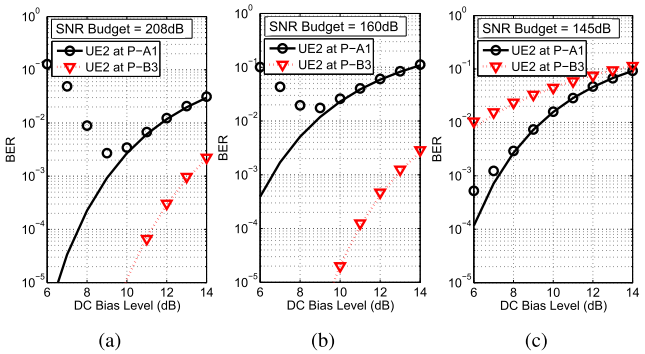

FIGURE 8. BER performances of the MU-MIMO-OOFDM-VLC systems employing NImR, ImR or mMMSV-PDS-ImR at various DC bias levels, where lines and markers denote the theoretical and simulated results, respectively. UE 1 fixed at PB-1; UE 2 fixed at P-A1 or P-B3. (a) NImR. (b) ImR. (c) mMMSV-PDS-ImR.

On the other hand, however, the impact from DC bias becomes more obvious when both UEs are close to each other, as indicated by the results represented by the round markers in Fig. 8. Note that since the BER performances of the NImR, ImR and mMMSV-PDS-ImR systems vary significantly, it is not possible to plot the BER curves of the various systems in a comparable range under the same SNR budget. Thus, in Fig. 8 we have assumed different SNR budgets for different systems, in order to present the results in a more readable manner. Since we are only interested in noting the gap between the theoretical and the simulated results in each individual system, assuming different SNR budgets does not affect our analysis in this regard.

More specifically, from Fig. 8(a) and Fig. 8(b), we observe that the simulated results of both the NImR and ImR systems become worse than their theoretical counterparts when the DC bias reduces below 10dB. This phenomenon implies that when the DC bias level becomes too low, although the available payload power budget is increased, the achievable system performance will become clipping-noise-limited rather than AWGN-limited. Such a phenomenon is due to the higher channel correlation created by the two closer UEs, which results in decreased MSVs for both UEs. As a consequence, the system then becomes more vulnerable to the negative impact of the clipping noise induced by a low DC bias level. Nonetheless, in such a hostile scenario, most parts of the theoretical and simulated performances of the proposed mMMSV-PDS-aided ImR system still agree, as shown in Fig. 8(c). It proves that in comparison to the conventional NImR and ImR benchmarkers, the mMMSV-PDS aided ImR system is capable of substantially mitigating the negative impact of the clipping noise induced by relative low DC bias levels, especially when two UEs are placed closely. Hence, the proposed scheme is much more robust than the conventional schemes, and provides a higher flexibility in system design to satisfy different illumination constraints associated with different DC bias values.

IV. CONCLUSIONS

In this paper, we have proposed a new PDS-aided MU-MIMO-OOFDM-VLC system invoking ImR. Through analytical and simulation results, it is shown that both the use of imaging lens and the employment of the PDS algorithm help to reduce MU-MIMO channel correlations. Furthermore, comprehensive performance comparisons have been conducted under different UE positions and DC bias levels, where it is found that the proposed mMMSV-PDS aided ImR system is capable of achieving good BER performances in most areas of the room compared with its counterpart schemes. This suggests that our design can be exploited to effectively reduce the MU-MIMO VLC channel correlations between PDs of the same or different UEs, which in turn offers a competent option for building MU-MIMO-OOFDM-VLC systems.

REFERENCES

[1] T. Komine and M. Nakagawa, "Fundamental analysis for visible-light communication system using LED lights," *IEEE Trans. Consum. Electron.*, vol. 50, no. 1, pp. 100–107, Feb. 2004.
[2] D. O'Brien *et al.*, "High-speed optical wireless demonstrators: Conclusions and future directions," *J. Lightw. Technol.*, vol. 30, no. 13, pp. 2181–2187, Jul. 1, 2012.
[3] S. Wu, H. Wang, and C. H. Youn, "Visible light communications for 5G wireless networking systems: From fixed to mobile communications," *IEEE Netw.*, vol. 28, no. 6, pp. 41–45, Nov. 2014.
[4] T. Fath and H. Haas, "Performance comparison of MIMO techniques for optical wireless communications in indoor environments," *IEEE Trans. Commun.*, vol. 61, no. 2, pp. 733–742, Feb. 2013.
[5] M. Jiang and L. Hanzo, "Multiuser MIMO-OFDM for next-generation wireless systems," *Proc. IEEE*, vol. 95, no. 7, pp. 1430–1469, Jul. 2007.
[6] C. Oestges, B. Clerckx, D. Vanhoenacker-Janvier, and A. J. Paulraj, "Impact of fading correlations on MIMO communication systems in geometry-based statistical channel models," *IEEE Trans. Wireless Commun.*, vol. 4, no. 3, pp. 1112–1120, May 2005.
[7] B. Clerckx and C. Oestges, "Space–time code design for correlated Ricean MIMO channels at finite SNR," *IEEE Trans. Signal Process.*, vol. 56, no. 9, pp. 4365–4376, Sep. 2008.
[8] N. Ishikawa and S. Sugiura, "Maximizing constrained capacity of power-imbalanced optical wireless MIMO communications using spatial modulation," *J. Lightw. Technol.*, vol. 33, no. 2, pp. 519–527, Jan. 15, 2015.
[9] A. Nuwanpriya, S.-W. Ho, and C. S. Chen, "Indoor MIMO visible light communications: Novel angle diversity receivers for mobile users," *IEEE J. Sel. Areas Commun.*, vol. 33, no. 9, pp. 1780–1792, Sep. 2015.
[10] A. Burton, Z. Ghassemlooy, S. Rajbhandari, and S.-K. Liaw, "Design and analysis of an angular-segmented full-mobility visible light communications receiver," *Trans. Emerg. Telecommun. Technol.*, vol. 25, no. 6, pp. 591–599, Mar. 2014.
[11] L. Zeng *et al.*, "High data rate multiple input multiple output (MIMO) optical wireless communications using white LED lighting," *IEEE J. Sel. Areas Commun.*, vol. 27, no. 9, pp. 1654–1662, Dec. 2009.
[12] P. M. Butala, H. Elgala, and T. D. C. Little, "Performance of optical spatial modulation and spatial multiplexing with imaging receiver," in *Proc. IEEE WCNC*, Apr. 2014, pp. 394–399.
[13] K. D. Dambul, D. C. O'Brien, and G. Faulkner, "Indoor optical wireless MIMO system with an imaging receiver," *IEEE Photon. Technol. Lett.*, vol. 23, no. 2, pp. 97–99, Jan. 2011.
[14] T. Q. Wang, Y. A. Sekercioglu, and J. Armstrong, "Analysis of an optical wireless receiver using a hemispherical lens with application in MIMO visible light communications," *IEEE J. Lightw. Technol.*, vol. 31, no. 11, pp. 1744–1754, Apr. 12, 2013.
[15] T. Chen, L. Liu, B. Tu, Z. Zheng, and W. Hu, "High-spatial-diversity imaging receiver using fisheye lens for indoor MIMO VLCs," *IEEE Photon. Technol. Lett.*, vol. 26, no. 22, pp. 2260–2263, Nov. 15, 2014.
[16] C. Chen, W. D. Zhong, D. Wu, and Z. Ghassemlooy, "Wide-FOV and high-gain imaging angle diversity receiver for indoor SDM-VLC systems," *IEEE Photon. Technol. Lett.*, vol. 28, no. 19, pp. 2078–2081, Oct. 1, 2016.

[17] H. Ma, L. Lampe, and S. Hranilovic, "Robust MMSE linear precoding for visible light communication broadcasting systems," in *Proc. IEEE Globecom Workshops (GC Wkshps)*, Dec. 2013, pp. 1081–1086.

[18] T. V. Pham, H. L. Minh, Z. Ghassemlooy, T. Hayashi, and A. T. Pham, "Sum-rate maximization of multi-user MIMO visible light communications," in *Proc. IEEE Int. Conf. Commun. Workshop (ICCW)*, Jun. 2015, pp. 1344–1349.

[19] B. Li, J. Wang, R. Zhang, H. Shen, C. Zhao, and L. Hanzo, "Multiuser MISO transceiver design for indoor downlink visible light communication under per-LED optical power constraints," *IEEE Photon. J.*, vol. 7, no. 4, pp. 1–15, Aug. 2015.

[20] J. Chen, Y. Hong, X. You, H. Zheng, and C. Yu, "Conceptual design of multi-user visible light communication systems over indoor lighting infrastructure," in *Proc. 9th Int. Symp. Commun. Syst., Netw. Digit. Signal Process. (CSNDSP)*, Jul. 2014, pp. 1154–1158.

[21] Y. Hong, J. Chen, Z. Wang, and C. Yu, "Performance of a precoding MIMO system for decentralized multiuser indoor visible light communications," *IEEE Photon. J.*, vol. 5, no. 4, Aug. 2013, Art. no. 7800211.

[22] Y. Hong, J. Chen, and C. Yu, "Performance improvement of the pre-coded multi-user MIMO indoor visible light communication system," in *Proc. CSNDSP*, Manchester, U.K., Jul. 2014, pp. 314–318.

[23] K. Cai and M. Jiang, "Multi-user MIMO-OOFDM imaging VLC system with PD selection," in *Proc. IEEE 83rd Veh. Technol. Conf. (VTC Spring)*, May 2016, pp. 15–18.

[24] Q. H. Spencer, A. L. Swindlehurst, and M. Haardt, "Zero-forcing methods for downlink spatial multiplexing in multiuser MIMO channels," *IEEE Trans. Signal Process.*, vol. 52, no. 2, pp. 461–471, Feb. 2004.

[25] H. Sung, S. R. Lee, and I. Lee, "Generalized channel inversion methods for multiuser MIMO systems," *IEEE Trans. Commun.*, vol. 57, no. 11, pp. 3489–3499, Nov. 2009.

[26] R. A. Horn and C. R. Johnson, *Matrix Analysis*. Cambridge, U.K.: Cambridge Univ. Press, 2012.

[27] S. D. Dissanayake and J. Armstrong, "Comparison of ACO-OFDM, DCO-OFDM and ADO-OFDM in IM/DD systems," *J. Lightw. Technol.*, vol. 31, no. 7, pp. 1063–1072, Apr. 1, 2013.

[28] B. Skalr, *Digital Communications: Fundamentals and Applications*. Upper Saddle River, NJ, USA: Prentice-Hall, 2001.

[29] P. Butala, H. Elgala, and T. Little, "SVD-VLC: A novel capacity maximizing VLC MIMO system architecture under illumination constraints," in *Proc. IEEE Globecom Workshops (GC Wkshps)*, Dec. 2013, pp. 1087–1092.

[30] R. Chen, R. W. Heath, and J. G. Andrews, "Transmit selection diversity for unitary precoded multiuser spatial multiplexing systems with linear receivers," *IEEE Trans. Signal Process.*, vol. 55, no. 3, pp. 1159–1171, Mar. 2007.

[31] R. W. Heath, S. Sandhu, and A. Paulraj, "Antenna selection for spatial multiplexing systems with linear receivers," *IEEE Commun. Lett.*, vol. 5, no. 4, pp. 142–144, Apr. 2001.

[32] D. Karunatilaka, F. Zafar, V. Kalavally, and R. Parthiban, "LED based indoor visible light communications: State of the art," *IEEE Commun. Surveys Tuts.*, vol. 17, no. 3, pp. 1649–1678, Aug. 2015.

[33] W. Li and M. Latva-Aho, "An efficient channel block diagonalization method for generalized zero forcing assisted MIMO broadcasting systems," *IEEE Trans. Wireless Commun.*, vol. 10, no. 3, pp. 739–744, Mar. 2011.

[34] J. Armstrong and B. Schmidt, "Comparison of asymmetrically clipped optical OFDM and DC-biased optical OFDM in AWGN," *IEEE Commun. Lett.*, vol. 12, no. 5, pp. 343–345, May 2008.

KUNYI CAI (S'16) received the B.Eng. degree in communication engineering from the School of Information Science and Technology, Sun Yat-sen University, Guangzhou, China, in 2015, where he is currently pursuing the M.Eng. degree. His research interests include visible light communications, multiuser communications, and the design of communication systems.

MING JIANG (M'07–SM'13) received the B.Eng. and M.Eng. degrees from the South China University of Technology, China, and Ph.D. degree from the University of Southampton, U.K., all in electronic engineering. He has substantial international and industrial experience with Fortune 500 telecom companies. From 2006 to 2013, he had held key R&D and/or management positions with Samsung Electronics Research Institute, U.K., Nortel's R&D Centre, China, and telecom equipment maker New Postcom, China, where he actively participated in numerous collaborative projects, including European FP6 WINNER-II, FP7 DAVINCI, WiMAX/IEEE802.16m, and LTE/LTE-A standardization, across the EU, North America and Asia, for researching and designing novel algorithms, telecommunication standards, radio access, and core network products. Since 2013, he has been a Full Professor and Ph.D. Supervisor with Sun Yat-sen University, China, where he focuses on both scientific research and technology transfer with industrial partners. His research interest falls into next-generation wireless mobile communications, including VLC, MIMO, OFDM, D2D, and HetNets. He has co-authored or contributed five Wiley books, 39 papers in prestigious international journals and conferences, 38 patents, and 400+ LTE/LTE-A/WiMAX standardization contributions. He is an IEEE Senior Member and was a recipient of several Chinese Council Awards in 2011, including Innovative Leading Talents, Outstanding Experts, and Top Overseas Scholars.

XIAO MA (M'08) received the Ph.D. degree in communication and information systems from Xidian University, China, in 2000. He is currently a Professor with the School of Data and Computer Science, Sun Yat-sen University, Guangzhou, China. From 2000 to 2002, he was a Post-Doctoral Fellow with Harvard University, Cambridge, MA, USA. From 2002 to 2004, he was a Research Fellow with the City University of Hong Kong. His research interests include information theory, channel coding theory and their applications to communication systems, and digital recording systems. He was a co-recipient with A. Kavčić and N. Varnica, of the 2005 IEEE Best Paper Award in signal processing and coding for data storage. In 2006, he received the Microsoft Professorship Award from Microsoft Research Asia.